1.5 μm dual-lateral-mode distributed Bragg reflector laser for terahertz excitation

Limgeng Zhang (张莉萌), Liqiang Yu (余力强), Biwei Pan (潘碧玮), Dan Lu (陆 丹)*, Jiaoqing Pan (潘教青), and Lingjuan Zhao (赵玲娟)**

Key Laboratory of Semiconductor Materials Science, Institute of Semiconductors, Chinese Academy of Science, and Beijing Key Laboratory of Low Dimensional Semiconductor Materials and Devices, Beijing 100083, China

**Corresponding author: ludan@semi.ac.cn; **corresponding author: ljzhao@semi.ac.cn*

Received September 29, 2015; accepted November 6, 2015; posted online December 21, 2015

A terahertz excitation source based on a dual-lateral-mode distributed Bragg reflector (DBR) laser working in the 1.5 μm range is experimentally demonstrated. By optimizing the width of the ridge waveguide, the fundamental and the first-order lateral modes are obtained from the laser. The mode spacing between the two modes is 9.68 nm, corresponding to a beat signal of 1.21 THz. By tuning the bias currents of the phase and DBR sections, the wavelengths of the two modes can be tuned by 2 nm, with a small strength difference (<5 dB) and a large side-mode suppression ratio (SMSR > 45 dB).

OCIS codes: 140.5960, 250.5960.
doi: 10.3788/COL201614.011406.

Sources at frequencies between 0.1 and 10 THz have applications in the medical fields, various measurement, nondestructive evaluation, security, wireless communications, and so on[1–6]. Over the past decades, there have been many technologies used to obtain terahertz radiation, including the electronics and photonics methods. A terahertz signal can be generated optoelectronically by using photoconductive antennas and femtosecond pulsed lasers[7]. However, such systems have drawbacks in their size and cost. Recently, a quantum cascade laser was proposed as a compact and continuous-wave (CW) terahertz source. However, the laser can barely work in room temperature, which limits its applications[8]. With its advantages of simplicity, low cost, and broad tuning range, beating of two optical modes on a photonic mixer is a promising method for CW-THz generation[9,10]. When two lasers with different wavelengths are detected by a photo-mixer, it is possible to generate terahertz radiation that corresponds to their wavelength separation. However, the beat source has been typically realized by two independent lasers, which inevitably meets problems in system stability. Alternatively, monolithically integrated dual-mode semiconductor lasers are an attractive solution for terahertz generation, due to their advantages in size, power consumption, possibilities of mass production, and integration possibilities with other optical components.

Up until now, much effort has been made to realize terahertz beat sources. Several monolithic laser structures have been demonstrated to emit two longitudinal modes simultaneously. A multi-section distributed feedback (DFB) laser has been proposed to provide a large frequency tuning range from tens of gigahertz to terahertz[11,12]. However, separate grating parameters are required to achieve wavelength detuning, which would result in a complicated fabrication process. The integration of two parallel DFB lasers is one of the most commonly used structures. In our previous work[13], two DFB lasers with a multimode interference coupler were demonstrated for tunable terahertz generation. It is very easy to realize a large tuning range, but a complicated fabrication process is needed to realize active–passive integration. Semiconductor lasers with an integrated feedback cavity can support two longitudinal modes simultaneously[14,15]. However, the generated mode spacings are usually below ∼100 GHz. Mode separation around the terahertz level is hard to realize with such a structure, due to the limitation of the length of the feedback cavity. More recently, a novel monolithic dual-lateral-modes beating DFB laser was proposed and demonstrated to generate a 150 GHz beat signal[16]. The simple fabrication processes make this device cost effective and suitable for mass production. However, the working wavelength of this laser is 1064 nm, which limits its application in hybrid fiber-terahertz communications. Also, the generated 150 GHz beating frequency is too low for many terahertz applications.

In this Letter, we demonstrate a 1.5 μm dual-lateral-mode distributed Bragg reflector (DBR) laser for terahertz mode beating. By taking advantage of the low-loss transmission window of the optical fiber, the two modes of the laser can be delivered to a photo-mixer located a long distance away, so as to realize a remote terahertz carrier transmission. It is also possible to integrate this device with other semiconductor devices, such as waveguide-type terahertz photo-mixers, semiconductor optical amplifiers, and electro-absorption modulators based on InP materials. Detailed simulations were carried out to investigate the effect of the ridge width on the generated beating frequency. By optimizing the width of the ridge waveguide, a 3.5 μm ridge was chosen to lower the optical confinement of the laser waveguide in the lateral direction and support both the fundamental mode and the first-order lateral mode. The generated two lateral modes had a mode

 © 2016 Chinese Optics Letters

spacing of 9.68 nm, corresponding to beating frequency of 1.21 THz. By adjusting the injected currents, the working wavelengths of the device can be tuned by 2 nm, and the beating frequency can be switched between 1.11 and 1.21 THz. Moreover, the power balance between the two modes was below 5 dB, and the side-mode suppression ratio (SMSR) is over 45 dB. Detailed investigations of this device, including near-field patterns, the spectral behavior, and autocorrelation characterization experiments, are reported.

The schematic illustration of the dual-lateral-mode ridge-waveguide DBR laser is shown in Fig. 1. This device consists of a gain section, a phase section, and a DBR grating section, with the lengths of 220, 100, and 150 μm, respectively. Traditional DBR lasers work in single longitudinal mode due to the existence of the DBR grating, as well as single lateral mode due to the ridge waveguide confinement in the lateral direction. The working wavelength of the device can be tuned by adjusting the bias currents of the phase and DBR sections. To realize dual-lateral-mode operation, the optical confinement in the lateral direction has to be adjusted. Due to the different propagation constants of the two lateral modes, the effective refractive index (EFI) of the two modes will result in different emission wavelengths (λ_0 and λ_{1st}). The beating of the two modes will generate a terahertz wave. We first investigated the ridge width by using commercial simulation software Crosslight PICs3D and the three-dimensional beam propagation method (3D BPM). The schematic diagram of the simulation structure is shown in Fig. 2, which shows a standard multi-quantum well (MQW) ridge waveguide laser. The simulation area was performed on the right half of the ridge for a symmetrical structure. The near-field pattern of the laser under different ridge widths (W) was investigated to find a proper ridge width to support dual-lateral-mode operation. The simulated results are shown in Fig. 3. The intensity of the near-field distribution is represented by a series of contour lines. In the figure, number 10 represents the strongest and number 1 represents the weakest intensity. The dotted line defines the ridge boundary. For this structure, when

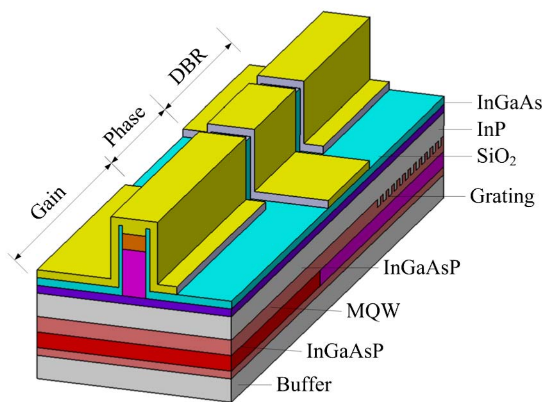

Fig. 1. Schematic diagram of the dual-mode DBR laser-packaged device.

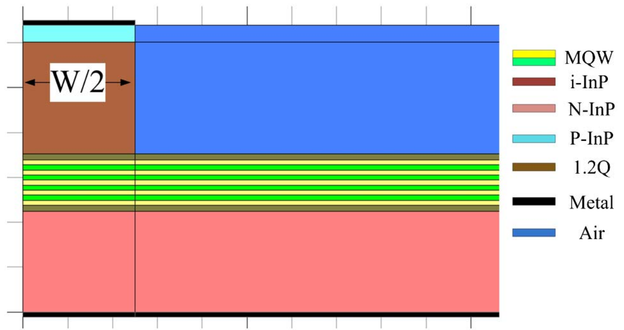

Fig. 2. Material structure schematic diagram of the ridge laser.

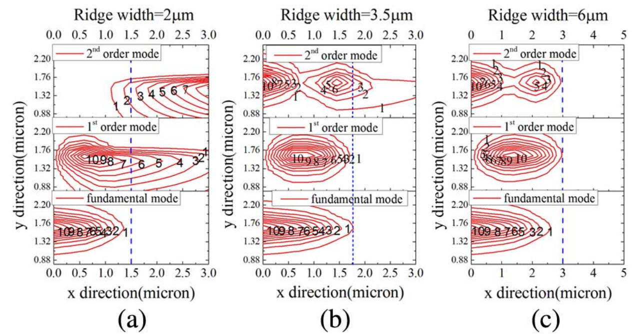

Fig. 3. Near-field mode pattern of the laser with (a) 2 μm ridge, supporting only the fundamental mode, (b) 3.5 μm ridge, supporting both the fundamental mode and the first-order mode, and (c) 6 μm ridge, supporting the fundamental mode, the first-order mode, and the second-order mode.

$W = 2$ μm, only the fundamental mode is supported. When $W = 3.5$ μm, the waveguide can support both the fundamental mode and the first-order mode simultaneously, while other higher-order mode are not supported. When $W = 6$ μm, the second-order mode will appear.

Two lateral modes with different EFIs would induce two Bragg wavelengths. To optimize the beating frequency, the EFIs of different modes as a function of the ridge width were investigated through 3D BPM. In the simulation, the material refractive indexes of 1.2Q InGaAsP and InP were set as 3.339 and 3.167, respectively, at a free space wavelength of 1.5 μm. Detailed parameters of each layer of the device module are listed in Table 1. The corresponding mode spacing can be obtained by

$$\lambda_0 - \lambda_{1st} = 2\Lambda(n_0 - n_{1st}), \tag{1}$$

where the grating period Λ was chosen to be 240 nm, λ_0 and λ_{1st} are the wavelengths of the fundamental mode and the first-order mode, respectively, and n_0 and n_{1st} are the modes' EFIs. By calculating the modes' EFIs of different ridge widths, the beating frequency of the fundamental mode, and the first-order mode as a function of ridge width can be plotted, as shown in Fig. 4. The beating frequency decreases from 1.02 to 0.4 THz when the ridge

Table 1. Detailed Parameters of Each Layer of the Device Module

Layer	Material	Thickness (nm)	Refractive Index
1	InP	2000	3.167
2	InGaAsP	120	3.339
3	MQWs	90	3.49
4	InGaAsP	120	3.339
5	InP	1800	3.167
6	InGaAs	200	3.482

width increases from 3.5 to 6 μm. Thus, a 3.5 μm ridge width is selected to get a higher beating frequency, as well as to obtain stable dual-mode lasing and suppress the higher modes.

Based on the above simulation analysis, a batch of devices was fabricated. The laser structure was grown by metal organic chemical vapor deposition in two steps. First, the epitaxial structure with five pairs of compressively strained InGaAsP MQW was grown on a S-doped n-type InP (100)-oriented substrate. A bandgap wavelength shift of 90 nm between the gain sections and the passive waveguide regions was realized by using quantum well intermixing technology. The DBR gratings were defined holographically on the grating region of the upper confinement hetero-junction (SCH) layer. The next epitaxial step was to grow a p-type cladding InP layer and a p-InGaAs contact layer on the upper SCH layer. By etching the p-InGaAs layer off and through He+ implantation, the electrical isolation process was accomplished. A Ti-Au metal layer was sputtered on the p-InGaAs contact layer to form a p-electrode. Then, the substrate was thinned, and the Au-Ge-Ni metal evaporated on the backside. The n-electrode was formed after rapid temperature annealing. Finally, a 3.5 μm ridge waveguide was formed by wet etching to support the first-order lateral mode.

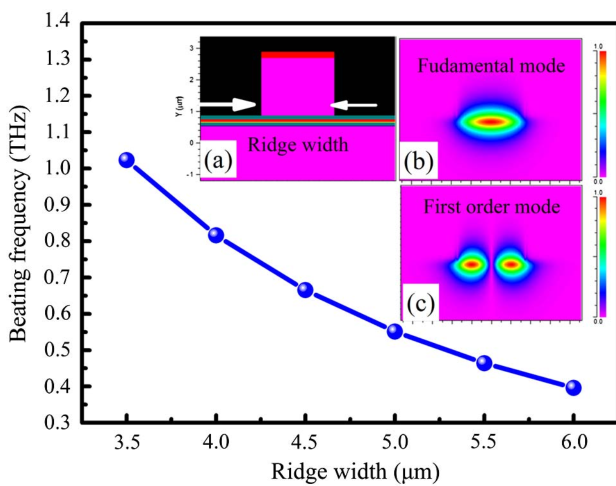

Fig. 4. Beating frequency of the fundamental mode and the first-order mode as a function of the ridge width. Inset (a) is the cross section of the material layers; (b) and (c) are the mode distributions of the fundamental mode and the first-order mode, respectively.

In the measurement, the cleaved device was mounted on a Cu heat sink, and the working temperature was maintained at 15°C by a thermoelectric cooler (TEC). The laser from the facet of the gain section was coupled out by a tapered single-mode fiber and monitored by an optical spectrum analyzer (Advantest Q8384) and an autocorrelator (A.P.E. pulse check).

First, the optical spectra and the near-field patterns were investigated. Figure 5 shows the wavelength distribution of this device when the current applied to the gain section changed from 40 to 180 mA, while the other sections were unbiased. When the device works in the stable single mode at a gain current smaller than 115 mA, the longitudinal mode spectrum shows a main emission peak with side modes. Figure 6(a) shows the typical optical spectrum of this state at a fixed gain current (I_{Gain}) of 100 mA, where a dominant single-longitudinal-mode laser at 1539 nm with an SMSR of 40 dB can be observed. With the further increasing of I_{Gain} beyond 115 mA, the first-order lateral mode appears. Figure 6(b) shows the optical spectrum of the dual-mode state at a 170 mA gain current. Two wavelengths at 1540 and 1530 nm correspond to the fundamental mode and the first-order lateral mode, respectively. The SMSRs of the two modes were both larger than 45 dB, and the intensity difference between them was less than 5 dB. Due to the Joule heating effect, the two working wavelengths shifted synchronously with a nearly fixed mode spacing with the increasing current.

To further verify the lasing mode state, the near-field distributions of different working states were characterized by an infrared CCD. The insets of Figs. 6(a) and 6(b) show the near-field intensity distribution of the fundamental mode state and the dual-mode state, respectively. The near-field pattern of the dual-mode state turned out to be fuzzy because the optical spots were mixed together when the two modes were exited simultaneously. To confirm that a terahertz signal was generated from this device

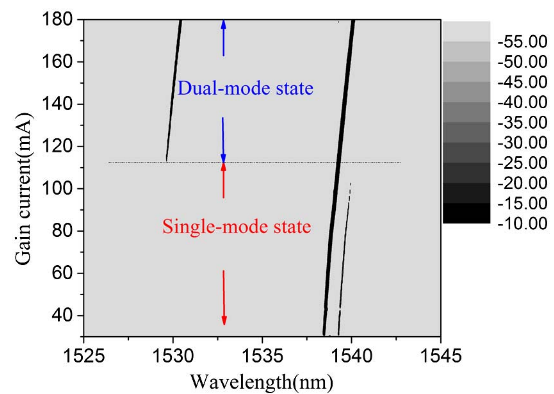

Fig. 5. Map of the output optical spectra when only the gain current was tuned.

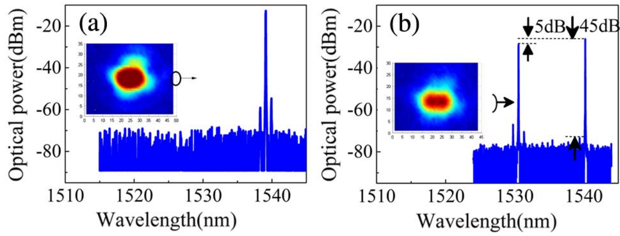

Fig. 6. (a) Typical output spectrum of the device in (a) the fundamental mode and (b) the dual-mode state. The insets show the near-field intensity distribution in (a) the fundamental mode operation state, and (b) the dual-lateral-mode operation state.

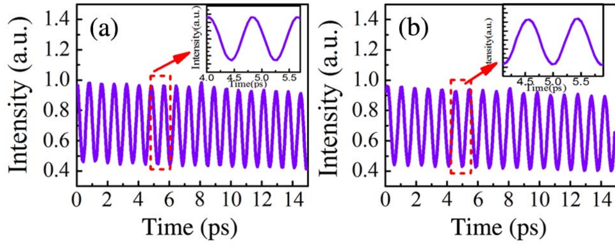

Fig. 7. (a) Autocorrelation trace of the device, where the wavelength difference between the two modes is 9.68 nm, corresponding to 1.21 THz at $I_{\mathrm{Gain}} = 140$ mA, $I_{\mathrm{Phase}} = 10$ mA. (b) Autocorrelation trace of the device, where the wavelength difference between the two modes is 8.88 nm, corresponding to 1.11 THz at $I_{\mathrm{Gain}} = 140$ mA, $I_{\mathrm{Phase}} = 20$ mA.

in the time domain, we measured the mode-beating pattern through an autocorrelator. Figure 7(a) shows the autocorrelation trace when the currents applied on the gain section and phase section (I_{Phase}) were 140 and 10 mA, respectively. The period of the signal was about 0.826 ps, corresponding to a beating frequency of 1.21 THz and a wavelength difference of 9.68 nm. When the phase current increased to 20 mA, the device showed another beating frequency, as seen in Fig. 7(b). The beating frequency was 1.11 THz, corresponding to an 8.88 nm wavelength difference. To further investigate the tuning characteristics, the beating frequencies as a function of the injection currents of the DBR section (I_{DBR}), at a fixed $I_{\mathrm{Gain}} = 140$ mA and $I_{\mathrm{Phase}} = 35$ mA are shown in Fig. 8(a). The corresponding peak wavelengths of the two modes are also plotted in Fig. 8(b). With the changing

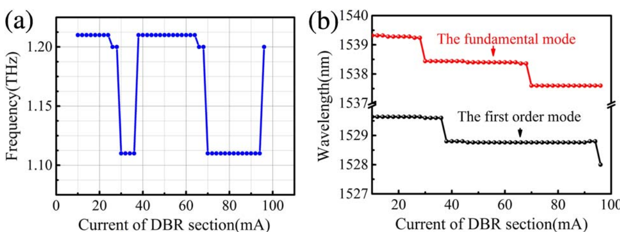

Fig. 8. Beating frequency (a) and corresponding peak wavelengths (b) as a function of the I_{DBR} with fixed $I_{\mathrm{Gain}} = 140$ mA, $I_{\mathrm{Phase}} = 35$ mA.

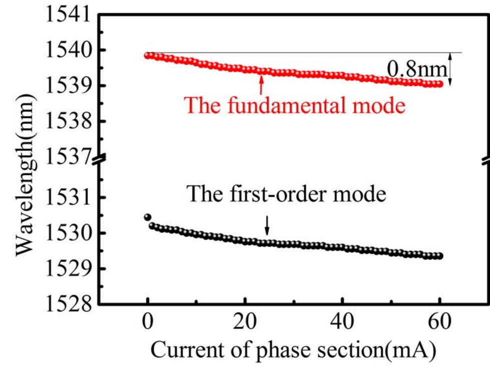

Fig. 9. Peak wavelengths as a function of I_{Phase} with fixed $I_{\mathrm{Gain}} = 140$ mA, $I_{\mathrm{DBR}} = 10$ mA.

of I_{DBR}, the two lateral modes show the same variation tendencies, which are similar to a traditional single-mode DBR laser. Due to the different mode hopping regions of the two wavelengths, two different beating frequencies of 1.21 and 1.11 THz can be obtained when adjusting the current injected into the DBR section, as shown in Fig. 8(b). The wavelengths of the two modes can be tuned by 2 nm, but with some mode hopping areas. By adjusting the phase and DBR currents, a continuous wavelength tuning can be obtained, as shown in Fig. 9. This feature could increase the flexibility of using this device when a specific wavelength channel is needed.

In conclusion, a dual-lateral-mode DBR laser as a terahertz excitation generator in the 1.5 μm range is designed and fabricated. Two wavelengths corresponding to two lateral modes are obtained in the 1.5 μm range. The mode-beating frequency can be switched between 1.11 and 1.21 THz by adjusting the bias currents of the device. Detailed investigations of this device, including the near-field pattern, the spectral behavior, and autocorrelation trace, are performed.

This work was supported by the National Natural Science Foundation of China (No. 61335009, 61274045, 61271066, 61321063), the National 973 Project of China (No. 2011CB301702), and the National 863 Project of China (No. 2013AA014202).

References

1. D. Saeedkia, *Handbook of Terahertz Technology for Imaging, Sensing and Communications* (Elsevier, 2013) pp. 91–117.
2. N. Oda, C. R. Phys. **11**, 496 (2010).
3. J. B. Jackson, M. Mourou, J. F. Whitaker, I. N. Duling III, S. L. Willimaon, M. Menu, and G. A. Mouron, Opt. Commun. **281**, 527 (2008).
4. Q. Zhou and X. Zhang, Chin. Opt. Lett. **9**, 110006 (2011).
5. J. Federici and L. Moeller, J. Appl. Phys. **107**, 111101 (2010).
6. N. Krumbholz, K. Gerlach, F. Rutz, M. Koch, R. Piesiewicz, T. Kürner, and D. Mittleman, Appl. Phys. Lett. **88**, 202905 (2006).
7. M. Tani, S. Matsuura, K. Sakai, and S.-i. Nakashima, Appl. Opt. **36**, 7853 (1997).
8. S. Fathololoumi, E. Dupont, C. Chan, Z. Wasilewski, S. Laframboise, D. Ban, A. Matyas, C. Jirauschek, Q. Hu, and H. C. Liu, Opt. Express **20**, 3866 (2012).

9. E. Brown, F. Smith, and K. McIntosh, J. Appl. Phys. **73**, 1480 (1993).
10. S. Matsuura, M. Tani, and K. Sakai, Appl. Phys. Lett. **70**, 559 (1997).
11. C. Zhang, S. Liang, L. Han, H. Zhu, and W. Wang, Opt. Lett. **38**, 3050 (2013).
12. N. Kim, J. Shin, E. Sim, C. W. Lee, D.-S. Yee, M. Y. Jeon, and Y. Jang, Opt. Express **17**, 13851 (2009).
13. M. Sun, S. Tan, F. Guo, S. Liu, D. Lu, and C. Ji, Lasers Optoelectron. Prog. **52**, 091302 (2015).
14. O. Brox, S. Bauer, M. Radziunas, M. Wolfrum, J. Sieber, J. Kreissl, B. Sartorius, and H. J. Wunsche, IEEE J. Quantum Electron. **39**, 1381 (2003).
15. B. Pan, L. Yu, D. Lu, L. Zhang, and L. Zhao, Chin. Opt. Lett. **12**, 110605 (2014).
16. A. Klehr, J. Fricke, A. Knauer, G. Erbert, M. Walther, R. Wilk, M. Mikulics, and M. Koch, IEEE J. S. Top. Quantum Electron. **14**, 289 (2008).